A Stability Analysis for Tethered Aerodynamically Shaped Balloons

JAMES D. DELAURIER*
G. T. Schjeldahl Company, Northfield, Minn.

This work investigates the dynamic stability of tethered, aerodynamically shaped balloons by considering the system to pose essentially a cable problem, with the balloon's dynamics giving end and auxiliary conditions. This physical model gives a first-order problem in a sequence of partial differential wave equations with nonhomogeneous boundary conditions. Further, these equations uncouple to give a "lateral" problem and a "longitudinal" problem—as in first-order airplane dynamics. The solution of either problem takes the form of a transcendental characteristic equation for the stability roots, from which these roots are extracted by using an electronic computer and a roots locus plot. Further, this theory was applied toward the development of a high-performance tethered balloon design, and the results showed that good stability was attainable by the use of large and aerodynamically efficient fins.

Introduction

IN 1915, Bairstow et al.,[1] while developing a theory for analyzing and predicting the stability of tethered balloons, discovered that an adequate mathematical representation leads to equations that are beyond the realm of easy solution by hand. Thus the design of stable tethered balloons so far has depended mostly on trial and error. However, interest in recent years in the use of tethered balloons as inexpensive station-keeping instrument platforms has again given rise to the need for an accurate stability theory. Further, with the use of the electronic computer, physical models even more complex than Bairstow's may now be handled with confidence.

A tethered balloon is physically and mathematically only a slight specialization of a general cable-body system, and, as such, there has been a fair amount of theoretical and experimental work on towed and tethered body stability. Most theories have used the approach of treating the cable-body system as being essentially a rigid-body dynamics problem, in which the cable is accounted for by force conditions at its body attachment point. These force conditions take the form of cable "stability derivatives," and are derived from the assumption that the cable is in an instantaneous equilibrium state with respect to certain of its end conditions. For instance, Glauert[2] based his analysis of a towed body on the cable end conditions of displacement. Similarly, Bryant et al.[3] used the same conditions for their analysis of tethered lifting bodies. One of the most sophisticated examples of this approach is given by Maryniak[10] in his study of towed glider stability, in which he considered conditions for a cable with tangential and normal aerodynamic forces. The cable stability derivative approach has the definite merit of giving linear ordinary differential equations with constant coefficients for describing the system's first-order behavior, from which detailed information on the system's motions may be obtained, as was done by Redd et al.[12] But such a physical model does not contain the basic mechanical nature of a cable-body system, especially if the time for a displacement "signal" to travel the length of the cable is of the same order of magnitude as the system's longest period—as may be the case for towed decelerators or high-altitude balloons. A more fundamental approach is to treat the system as a cable problem in which the body supplies certain end conditions. This physical model is much more general, and contains the previous mode of analysis as a special case. Basing his analysis on this approach, DeLaurier[4, 5] obtained a solution for the first-order stability of a cable-body system, and verified this solution with experiments. This theory has since been used for the stability analysis of tethered balloons, and the balance of this article is devoted toward elucidating the theory and its application.

Received August 12, 1971; revision received May 8, 1972.
Index categories: Aircraft Performance; Aircraft Handling, Stability, and Control.

* Staff Engineer, Advanced Programs Division. Member AIAA.

Theoretical Stability Analysis

Types of Tethered Balloon Stability

As an important preliminary to this paper, one must note that limit-cycle oscillations are a characteristic of systems which have mechanical constraints on their moving components, such as cable-body systems; further, such systems may have first-order instability, but likewise have limit-cycle stability. This is in direct contrast to free systems such as airplanes, where first-order instability, if uncorrected, almost always leads to complete disruption of the system's original steady motion. However, first-order stability for a free-flying vehicle, even with nonfirst-order disturbances, almost always guarantees its stability. This is also true for a cable-body system. Thus one sees that a first-order stability analysis on cable-body systems is necessarily conservative and is thereby of considerable value toward designing a strongly stable system.

Equations of Motion

As mentioned in the Introduction, the physical model for this analysis has been to consider the cable-body system as being essentially a cable problem, in which the body provides end and auxiliary conditions. To this end, the equations of motion for a cable segment were derived based on the following assumptions: 1) The cable segment has uniform density and geometry along its length. 2) The segment is perfectly flexible and inextensible. 3) The segment has a cross section that is round, or nearly so—such as stranded wire. 4) The segment is totally immersed in a homogeneous uniform fluid stream. 5) The Reynolds number of the segment's crossflow is subcritical. 6) The cable segment is nearly straight over its entire length. 7) The magnitude of the segment's perturbed displacement is small compared with its length. 7) The magnitude of the segment's perturbed velocity is small compared with the freestream velocity. 9) The segment's equilibrium tension is nearly uniform and linear along its length, and is large compared with the perturbed tension contribution.

Thus, according to these assumptions, the equations of motion for the segment are

$$D^2\tilde{\xi} - C^2(\partial^2\tilde{\xi}/\partial\tilde{s}^2) - k_1 D\tilde{\zeta} - k_2(\partial\tilde{\zeta}/\partial\tilde{s}) = 0 \quad (1)$$

$$D^2\tilde{y} - C^2(\partial^2\tilde{y}/\partial\tilde{s}^2) + k_6 D\tilde{y} + k_7(\partial\tilde{y}/\partial\tilde{s}) = 0 \quad (2)$$

$$D^2\tilde{\zeta} - C^2(\partial^2\tilde{\zeta}/\partial\tilde{s}^2) + k_3 D\tilde{\zeta} + k_4(\partial\tilde{\zeta}/\partial\tilde{s}) = 0 \quad (3)$$

where C, k_1 through k_7 = nondimensional constants involving the cable segment's physical, aerodynamic, and geometrical properties; $\tilde{\xi}$, $\tilde{y}$, and $\tilde{\zeta}$ = nondimensional perturbation values of the cable's coordinates (see Fig. 1); $\tilde{s}$ = nondimensional cable length coordinate; and $D(\,)$ and $D^2(\,)$ = nondimensional time derivatives.

Now, in order to treat a cable with a general curvature and tension variation, an important concept was introduced: the complete cable may be dynamically represented by a number of the first-order segments—each joined one to the next by matching conditions of displacement and slope. Mathematically, this means that the general cable is divided into n segments, where the segment lengths are chosen short enough such that the assumptions, 1–9, could be considered to apply to each. Further, a given segment i is matched to the next segment $i+1$ by the conditions

$$L_i\tilde{\zeta}_i(1,\hat{t}) = L_{i+1}\tilde{\zeta}_{i+1}(0,\hat{t}) \quad (4)$$

$$L_i\tilde{y}_i(1,\hat{t}) = L_{i+1}\tilde{y}_{i+1}(0,\hat{t}) \quad (5)$$

$$(\partial\tilde{\zeta}_i/\partial\tilde{s}_i)(1,\hat{t}) = (\partial\tilde{\zeta}_{i+1}/\partial\tilde{s}_{i+1})(0,\hat{t}) \quad (6)$$

$$(\partial\tilde{y}_i/\partial\tilde{s}_i)(1,\hat{t}) = (\partial\tilde{y}_{i+1}/\partial\tilde{s}_{i+1})(0,\hat{t}) \quad (7)$$

where $i = 1, 2, \ldots, n-1$; L_i = length of cable segment; and $\hat{t}$ = nondimensional time.

Also, note that for the fixed end condition of the first segment, one has

$$\tilde{\zeta}_1(0,\hat{t}) = 0 \quad (8)$$

$$\tilde{y}_1(0,\hat{t}) = 0 \quad (9)$$

Further, end conditions of the last segment $i = n$ are given by the body's equations of motion. These equations were derived subject to the following assumptions: 1) The body is rigid. 2) The body is completely immersed in a homogeneous fluid stream. 3) The body is symmetric with respect to the $\mathbf{n}_1$, $\mathbf{n}_3$ plane (see Fig. 2). 4) The cable is free to pivot at the attachment point. 5) The magnitude of the body's perturbed rotations is small. 6) The magnitude of the body's angular velocities is small compared with the ratio of the freestream velocity divided by the body characteristic length. 7) The magnitude of the body's perturbed velocities is small compared with the freestream velocity. 8) Aerodynamic effects may be represented by the concept of stability derivatives. The resulting equations, which are derived at length in Refs. 4 and 5, are given in the Appendix.

Now, when the body equations are rearranged, the cable contribution terms are either eliminated or isolated, and these

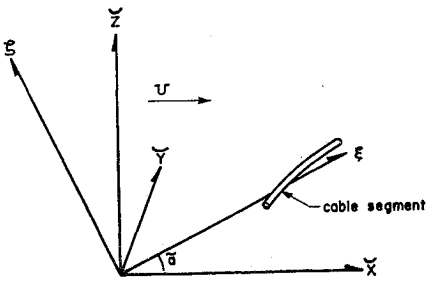

Fig. 1 Cable coordinate system.

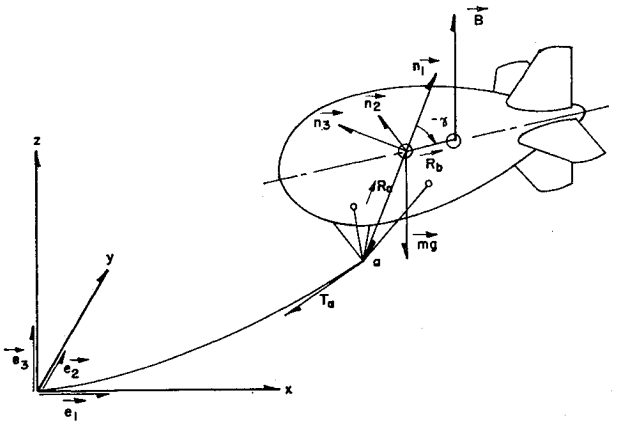

Fig. 2 Body coordinate system.

equations are thus put into their most convenient form for use as end conditions and auxiliary conditions

$$(\partial\tilde{\zeta}/\partial\tilde{s})(1,\hat{t}) = (\pi_{40}D^2 + \pi_{41}D)\tilde{\zeta}(1,\hat{t}) + (\pi_{42}D^2 + \pi_{43}D + \pi_{44})\tilde{\theta} \quad (10)$$

$$(\partial\tilde{y}/\partial\tilde{s})(1,\hat{t}) = (\pi_{57}D^2 + \pi_{58}D)\tilde{y} + (\pi_9 D + \pi_{10})\tilde{\varphi} + (\pi_{59}D^2 + \pi_{60}D + \pi_{12})\tilde{\psi} \quad (11)$$

$$(\pi_{45}D^2 + \pi_{46}D)\tilde{\zeta}(1,\hat{t}) + (\pi_{47}D^2 + \pi_{48}D + \pi_{33})\tilde{\theta} = 0 \quad (12)$$

$$(\pi_{49}D^2 + \pi_{50}D)\tilde{y}(1,\hat{t}) + (-i_{xz}D^2 + \pi_{23}D + \pi_{24})\tilde{\varphi} + (\pi_{51}D^2 + \pi_{52}D + \pi_{27})\tilde{\psi} = 0 \quad (13)$$

$$(\pi_{53}D^2 + \pi_{54}D)\tilde{y}(1,\hat{t}) + [(C_{la1} - i_{xx})D^2 + C_{lp}D - C_{lv}\sin\theta_0 + \hat{R}\hat{B}\sin\gamma\cos\theta_0]\tilde{\varphi} + (\pi_{55}D^2 + \pi_{56}D + C_{lv})\tilde{\psi} = 0 \quad (14)$$

where π_{23} through π_{60} = nondimensional constants involving the coefficients of the body equations.

These equations, along with the cable and matching Eqs. (1–9), constitute a completely posed boundary-value problem for the system's motion. Moreover, note that the lateral motion and the longitudinal motion are uncoupled in this first-order analysis; that is, the equations for $\tilde{y}$, $\tilde{\psi}$ and $\tilde{\varphi}$ are a complete set, as are those for $\tilde{\zeta}$ and $\tilde{\theta}$. Thus, the system's longitudinal stability may be solved for, separate from its lateral stability.

Solution of the Stability Equations

The boundary-value problem for the longitudinal stability modes is defined by the cable Eq. (3), along with the end conditions, Eqs. (4, 6, 8, and 10), and the auxiliary condition, Eq. (12). Thus, one must deal with a sequence of homogeneous partial differential wave equations with nonhomogeneous end conditions, which is considerably more complicated than the set of homogeneous ordinary differential equations of airplane stability analysis.[6] However, drawing on the nonhomogeneous partial differential equation techniques in Berg and McGregor,[2] one may obtain a formal solution by the method of separation of variables. Further, noting that all equations are linear and have constant coefficients, one then assumes a perturbed harmonic motion. Thus,

$$\tilde{\zeta}_i(\tilde{s}_i,\hat{t}) = Z_i(\tilde{s}_i)\exp(\sigma\hat{t}),\ i = 1, 2, \ldots, n \quad (15)$$

Upon substituting this into the cable Eq. (3), and matching according to the end conditions, Eqs. (4, 6, and 8), one obtains

$$Z_i(\tilde{s}_i) = (Z_i)_1 \exp(\Lambda_i\tilde{s}_i)\,[\exp(\Omega_i\tilde{s}_i) - Q_i\exp(-\Omega_i\tilde{s}_i)] \quad (16)$$

where

$$Q_1 = 1 \quad (17)$$

$$Q_i = \frac{\left\{\frac{L_i}{L_{i-1}}\left[\Lambda_{i-1}+\Omega_{i-1}\left(\frac{\exp(\Omega_{i-1})+Q_{i-1}\exp(-\Omega_{i-1})}{\exp(\Omega_{i-1})-Q_{i-1}\exp(-\Omega_{i-1})}\right)\right]-\Lambda_i-\Omega_i\right\}}{\left\{\frac{L_i}{L_{i-1}}\left[\Lambda_{i-1}+\Omega_{i-1}\left(\frac{\exp(\Omega_{i-1})+Q_{i-1}\exp(-\Omega_{i-1})}{\exp(\Omega_{i-1})-Q_{i-1}\exp(-\Omega_{i-1})}\right)\right]-\Lambda_i+\Omega_i\right\}}$$

$$(i = 2, 3, \ldots, n) \qquad (18)$$

$$\Lambda_i = \frac{(k_4)_i}{2C_i^2}, \qquad \Omega_i = \left[\Lambda_i^2 + \frac{\sigma^2 + (k_3)_i\sigma}{C_i^2}\right]^{1/2}$$

and $(Z_i)_1$ is a constant.

Now, in the spirit of the harmonic analysis, assume that

$$\theta = \Theta \exp(\sigma t) \qquad (19)$$

where Θ is a constant. Substituting this and Eqs. (15–18) into the end and auxiliary conditions, Eqs. (10) and (12), for the last segment $i = n$ one obtains the following transcendental equations:

$$\exp(\Lambda_n)[\exp(\Omega_n) - Q_n\exp(-\Omega_n)] \times \left\{\pi_{40}\sigma^2 + \pi_{41}\sigma - \Lambda_n - \Omega_n\left[\frac{\exp(\Omega_n) + Q_n\exp(-\Omega_n)}{\exp(\Omega_n) - Q_n\exp(-\Omega_n)}\right]\right\} \times (Z_n)_1 + (\pi_{42}\sigma^2 + \pi_{43}\sigma + \pi_{44})\Theta = 0 \qquad (20)$$

$$\exp(\Lambda_n)[\exp(\Omega_n) - Q_n\exp(-\Omega_n)](\pi_{45}\sigma^2 + \pi_{46}\sigma)(Z_n)_1 + (\pi_{47}\sigma^2 + \pi_{48}\sigma + \pi_{33})\Theta = 0 \qquad (21)$$

These equations are two linear homogeneous equations in $(Z_n)_1$ and Θ. Thus, it follows that an equation for σ (characteristic equation) may be obtained by putting Eqs. (20) and (21) into a determinant, and setting it equal to zero.

The characteristic determinant for the lateral stability roots may be found in a similar fashion. Starting from the boundary-value problem as defined by the cable Eq. (2), the end conditions Eqs. (5, 7, 9, and 11), and the auxiliary conditions, Eqs. (13) and (14), one may proceed in a similar fashion as for the longitudinal case. To this end, a harmonic solution for y_i is assumed

$$\tilde{y}_i(\tilde{s}_i,\hat{t}) = Y_i(\tilde{s}_i)\exp(\lambda\hat{t}), \qquad i = 1, 2, \ldots, n \qquad (22)$$

Upon substituting this into the cable Eq. (2), and matching according to the end conditions, Eqs. (5, 7, and 9), one obtains

$$Y_i(\tilde{s}_i) = (Y_i)_1 \exp(\Gamma_i\tilde{s}_i)[\exp(\Delta_i\tilde{s}_i) - P_i\exp(-\Delta_i\tilde{s}_i)] \qquad (23)$$

where

$$P_1 = 1 \qquad (24)$$

$$P_i = \frac{\left\{\frac{L_i}{L_{i-1}}\left[\Gamma_{i-1}+\Delta_{i-1}\left(\frac{\exp(\Delta_{i-1})+P_{i-1}\exp(-\Delta_{i-1})}{\exp(\Delta_{i-1})-P_{i-1}\exp(-\Delta_{i-1})}\right)\right]-\Gamma_i-\Delta_i\right\}}{\left\{\frac{L_i}{L_{i-1}}\left[\Gamma_{i-1}+\Delta_{i-1}\left(\frac{\exp(\Delta_{i-1})+P_{i-1}\exp(-\Delta_{i-1})}{\exp(\Delta_{i-1})-P_{i-1}\exp(-\Delta_{i-1})}\right)\right]-\Gamma_i+\Delta_i\right\}}$$

$$(i = 2, 3, \ldots, n) \qquad (25)$$

$$\Gamma_i = (k_7)_i/2C_i^2, \quad \Delta_i = [\Gamma_i^2 + (\lambda^2 + (k_6)_i\lambda)/C_i^2]^{1/2}$$

and $(Y_i)_1$ is a constant.

Further, consistent with the harmonic assumption, Eq. (22), assume that

$$\tilde{\psi} = \Psi\exp(\lambda\hat{t}) \quad \text{and} \quad \tilde{\varphi} = \Phi\exp(\lambda\hat{t}) \qquad (26)$$

where Ψ and Φ are constants. Substituting this, and Eqs. (23–25) into the end and auxiliary conditions for the last segment $i = n$ one obtains three linear, homogeneous equations in $(Y_n)_1$, Ψ, and Φ. Again, as with the longitudinal case, these may be set into a determinant to yield the characteristic equation for λ.

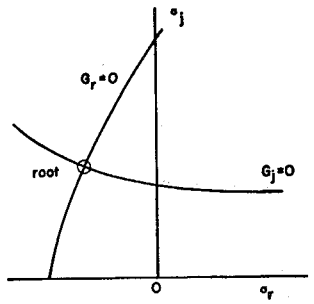

Fig. 3 Typical longitudinal roots locus plot.

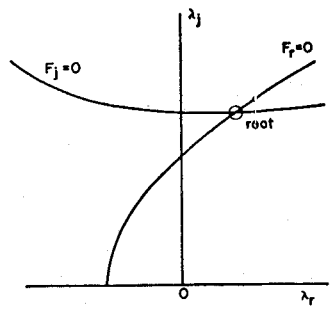

Fig. 4 Typical lateral roots locus plot.

Note that the characteristic roots σ and λ are, in general, complex

$$\sigma = \sigma_r + j\sigma_j \quad \text{and} \quad \lambda = \lambda_r + j\lambda_j, \quad \text{where } j = (-1)^{1/2} \qquad (27)$$

Thus, the characteristic equations are transcendental and complex, and there is no general closed form solution for the roots. Therefore, a graphical root extraction method was used, namely, roots locus plots. To implement this, Eq. (27) was substituted into the characteristic equations, and then expanded into real and imaginary parts. The characteristic equations then took the form

$$G_r(\sigma_r,\sigma_j) + jG_j(\sigma_r,\sigma_j) = 0 \qquad (28)$$

$$F_r(\lambda_r,\lambda_j) + jF_j(\lambda_r,\lambda_j) = 0 \qquad (29)$$

where $G_r(\sigma_r,\sigma_j)$ and $F_r(\lambda_r,\lambda_j)$ are the real parts of the characteristic equations, and $G_j(\sigma_r,\sigma_j)$ and $F_j(\lambda_r,\lambda_j)$ are the imaginary parts of the characteristic equations.

This then forms the basis for the roots locus plot, in that, first, the root pair is sequenced through a range of values, and for each of these values, the real and imaginary part of the characteristic equation is calculated. Next, for each root pair for which either the real part or the imaginary part of the equation equals zero, this root pair is marked on a coordinate system. These points then define curves for which either the real or the imaginary part of the characteristic equation equals zero, and the intersection of these curves then defines the characteristic roots. Examples of roots locus plots are shown in Figs. 3 and 4 for longitudinal and lateral cases, respectively.

Application of the Theory

The theory was compared with wind-tunnel experiments on a kite[5] and a suspended finned body.[4] For both cases, theory and experiment compared very well, and it was thus felt that the theory was sufficiently verified so that it could be directed toward its primary purpose, the prediction of a cable-body system's stability characteristics. The system, in this case, is a tethered balloon, shown in Fig. 5. Note that its characteristic length b is the hull length, and the characteristic area is the hull volume to the 2/3 power, i.e.

$$b = 138.0 \text{ ft and } S = (2.0 \times 10^5)^{2/3} = 3420.0 \text{ ft}^2 \qquad (30)$$

Further, the balloon's inertial properties were found from finite element computation, based on the measured masses of

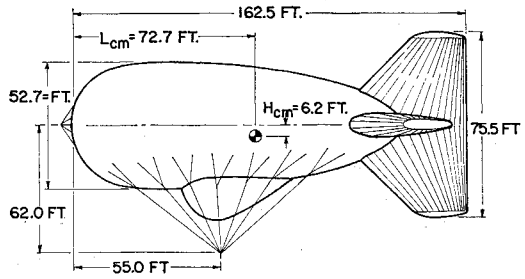

Fig. 5 Tethered balloon layout.

the component parts. Since the enclosed air and helium change their density and mass center location with altitude, their contribution to the inertial properties had to be calculated for each cable length and wind speed combination. For example, the total inertial properties when cable length L equals 4000 ft and wind speed U equals 20 fps are m = total balloon mass = 386.5 slugs; I_{xx} = moment of inertia about the x axis = 8.906×10^4 slug-ft^2; I_{yy} = moment of inertia about the y axis = 4.7801×10^5 slug-ft^2; I_{zz} = moment of inertia about the z axis = 4.2255×10^5 slug-ft^2; I_{xz} = product of inertia with respect to the $x-z$ axes = 5.681×10^4 slug-ft^2, where the mass center location (see Fig. 5) is

$$L_{cm} = 72.65 \text{ ft and } H_{cm} = -6.16 \text{ ft} \tag{31}$$

As for the cable, it is a smoothjacketed NOLARO line (manufactured by the Columbian Rope Company) with the following properties: R = radius = 0.0323 ft; $\bar{\rho}$ = mass/length = 0.00621 slug/ft, and its aerodynamic coefficients are obtained from Hoerner[9]

$$C_{ao} = \text{zero angle drag coefficient} = 0.035$$
$$K = \text{cross-sectional drag coefficient} = 1.19 \tag{32}$$

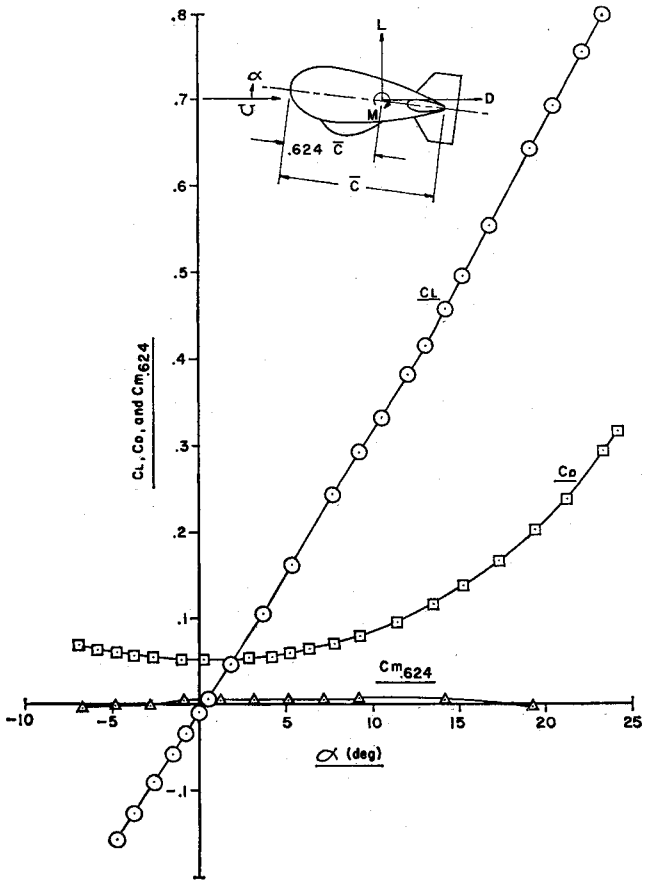

Fig. 6 Tethered balloon aerodynamic characteristics.

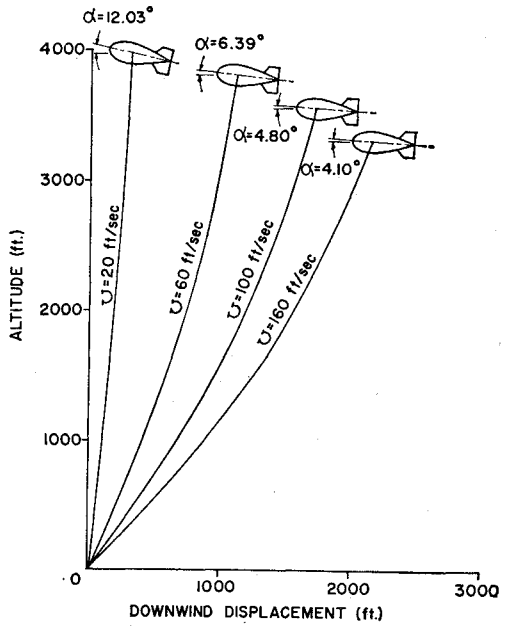

Fig. 7 Cable-balloon system equilibrium configuration.

Next, the system's equilibrium configuration was found from theory. For the balloon itself, wind-tunnel tests on a rigid model[8] gave the aerodynamic inputs (see Fig. 6) for the force and moment balance equations, which, through an iterative computer solution, gave the balloon's angle-of-attack α as a function of its altitude and wind speed. Further, the cable equilibrium equations were solved by a finite difference method, as described in Ref. 4, to yield the cable profile and tension variation. Thus, by coupling the balloon and cable equilibrium solutions together it was possible to solve for the entire system's equilibrium configuration as a function of cable length and wind speed. An example of this result for $L = 4000$ ft is shown in Fig. 7.

Now, the stability derivatives were found from a combination of experiment[8] and theory.[4,11,13] Since the balloon's mass center and angle-of-attack are functions of the wind speed and cable length, the derivatives were written in a very functional form, and values were calculated for each given situation. For example, the longitudinal stability derivatives for $L = 4000$ ft and $U = 20$ fps are

$$(C_{Xu})_0 = 0, \quad (C_{Xa1})_0 = -0.24, \quad (C_{Zu})_0 = 0, \quad (C_{Za1})_0 = 0$$
$$(C_{mu})_0 = 0, \quad (C_{ma1})_0 = 0.0156, \quad (C_{Xw})_0 = -0.070, \quad (C_{Xa3})_0 = 0$$
$$(C_{Zw})_0 = -1.967, \quad (C_{Za3})_0 = -1.32, \quad (C_{mw})_0 = -0.189$$
$$(C_{ma3})_0 = 0.121, \quad (C_{Xq})_0 = 0, \quad (C_{Zq})_0 = -1.037$$
$$(C_{m\alpha 2})_0 = -0.089, \quad (C_{mq})_0 = -0.353 \tag{33}$$

where the subscript $(\ )_0$ denotes values taken with respect to the wind-aligned body-fixed axes of usual airplane convention (see pp. 103–104 of Ref. 6).

Also, the lateral stability derivatives for $L = 4000$ ft and $U = 20$ fps are

$$(C_{Yv})_0 = -1.91, \quad (C_{Ya2})_0 = -1.32, \quad (C_{nv})_0 = 0.117$$
$$(C_{na2})_0 = -0.121, \quad (C_{lv})_0 = -0.090, \quad (C_{la2})_0 = -0.086$$
$$(C_{Yr})_0 = 1.264, \quad (C_{nr})_0 = -0.533, \quad (C_{n\alpha 3})_0 = -0.089$$
$$(C_{lr})_0 = 0.0271, \quad (C_{Yp})_0 = 0.133, \quad (C_{np})_0 = -0.056$$
$$(C_{lp})_0 = -0.096, \quad (C_{la1})_0 = -0.006 \tag{34}$$

The geometrical, inertial, and aerodynamic information contained in Figs. 5, 6, and 7 and the data in Eqs. (30–34) provided the necessary inputs to the stability analysis, and the results are shown in Figs. 8–11. Of all the stability modes

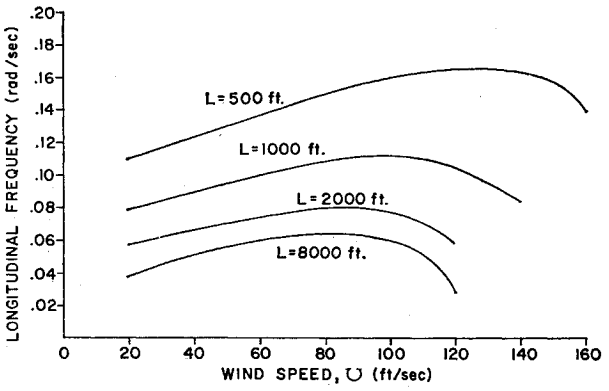

Fig. 8 System longitudinal frequency of oscillation.

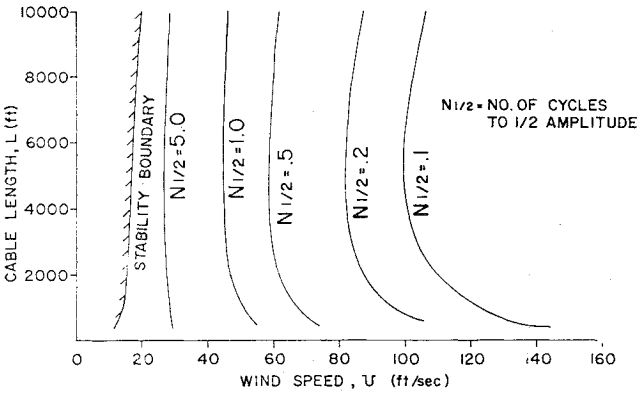

Fig. 10 Longitudinal stability map.

given by the theory, there was consistently one dominant least stable mode whose frequency was of the order of magnitude of the "pendulum" frequency

$$\text{pendulum frequency (rad/sec)} \cong (\text{cable tension at body})^{1/2}/mL$$

This result was confirmed by experimental observation in Refs. 4 and 5. Therefore, the characteristics of this mode only, are shown in the results.

Considering, first, the frequency plots (Figs. 8 and 9), one sees that these generally follow the trend of increasing frequency with increasing U and decreasing L. The exception occurs at the high values of U in the longitudinal plot. For this case, theory predicts such strong stability with increasing wind speed that the motion approaches the critically damped situation in which oscillation entirely disappears. Otherwise, the lateral and longitudinal frequency plots are very similar. This is not the case for the stability maps.

Noting, first, the longitudinal stability map, Fig. 10, one sees that the system is stable throughout most of the region considered. However, there exists a narrow region of instability at $0 < U < 20$ fps for all cable lengths. This is due primarily to an interaction between the balloon's lift and drag, where the lift acts as a forcing function and the drag acts as a damping function, and thereby, a high lift/drag ratio aggravates the situation, as with airplane "phugoid" oscillations. Further, this type of motion was experimentally observed in Ref. 5.

Nevertheless, a high lift/drag ratio is highly desired for a tethered balloon's over-all performance. Moreover, the small unstable region is predicted by a conservative first-order theory, which precludes the fact that experience with tethered balloons[12] indicates that only limit cycle oscillations will occur, thus making this region, for operational purposes, acceptably stable.

The lateral stability map (Fig. 11) shows the system to be stable throughout the entire range of wind speeds and cable lengths considered, which is considerably more stable lateral behavior than is usually the case with finned axisymmetric bodies.[4] This is due greatly to the balloon's large, efficiently shaped vertical fins. Although a cable-body system's dynamic stability is governed by a complicated interaction of its physical and aerodynamic properties, strong contributions to a finned balloon's stability are given by large positive values of the yawing derivative $(C_{nv})_0$ and large negative values of the side-slip and rotary yawing derivatives $(C_{Yv})_0$ and $(C_{nr})_0$ respectively. A large and properly designed vertical fin enhances these values, and this consideration gave rise to the fin design of this balloon.

Conclusions

Within the limits of the theory's assumptions, it is felt that this stability analysis provides a reasonable method for predicting the first-order motion of tethered, aerodynamically shaped balloons, as well as that for a variety of other cable-body systems, as evidenced by Refs. 4 and 5. Because the general cable equations of motion were considered, one need not place any restrictions on the cable's first-order motion; i.e., no "instantaneous equilibrium" physical model is assumed, such as in Ref. 3. Thus, this theory may be applied readily to systems in which the time of displacement signal propagation along the cable length is of the same order of magnitude as, or greater than, the system's largest period of oscillation. Examples of such systems include towed reentry decelerators, as well as high-altitude balloons.

The essential feature of the theory is that the cable-body system is treated as a segmented cable problem, where the body provides end and auxiliary conditions for the last segment. This physical model can readily lend itself to some

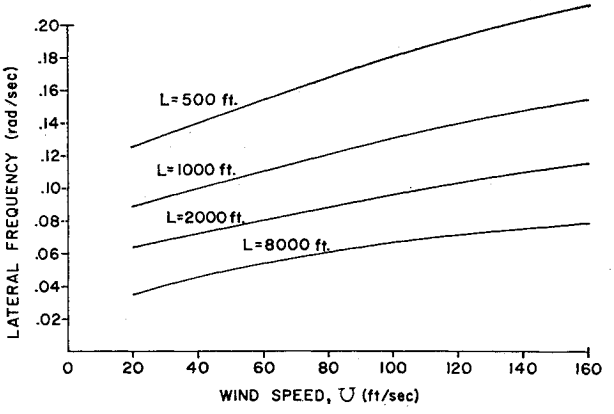

Fig. 9 System lateral frequency of oscillation.

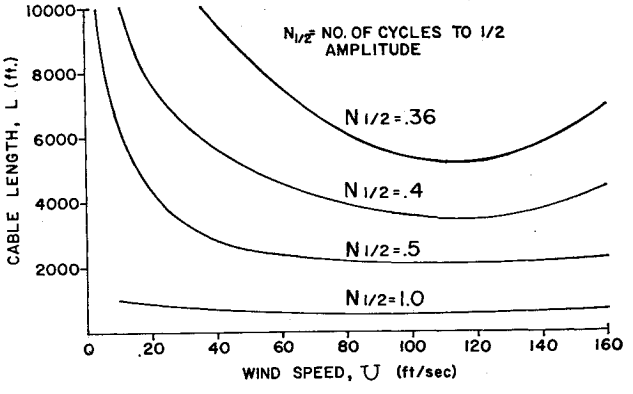

Fig. 11 Lateral stability map.

interesting applications. For instance, the problem of two bodies connected by a cable may be treated by replacing the fixed end conditions at the first segment with a set of body-derived end and auxiliary conditions, similar to those for the last segment. Finally, another application would be to consider a finite body midway along the cable. In this case, the end conditions on the two adjacent cable segments are found from the equations of motion of the midcable body.

Appendix: The Body Equations of Motion

From Refs. 4 and 5, the body's equations of motion are

$$\{[(C_{Xa1}-\mu)\cos\theta_0 + C_{za3}\sin\theta_0]\,D^2 + (C_{Xu}\cos\theta_0 + C_{Xw}\sin\theta_0)\,D\}\hat{x} +$$
$$\{[C_{Xa3}\cos\theta_0 - (C_{Xa1}-\mu)\sin\theta_0]\,D^2 + (C_{Xw}\cos\theta_0 - C_{Xu}\sin\theta_0)\,D\}\,\hat{z} +$$
$$\{C_{Xq}D - \cos\theta_0\,[C_{Xw} + (\hat{B}-\widehat{mg}) - \hat{T}_0\,(\partial\bar{z}/\partial s)_a] + \hat{T}_0\,(\partial\bar{x}/\partial s)_a\sin\theta_0\}\,\tilde{\theta} +$$
$$\hat{T}_0[(\partial\bar{z}/\partial s)_a\sin\theta_0 - (\partial\bar{x}/\partial s)_a\cos\theta_0] = 0 \qquad \text{(A1)}$$

$$[(C_{Ya2}-\mu)D^2 + C_{Yv}D]\,\hat{y} + [(\cos\theta_0\,C_{Yr} - \sin\theta_0\,C_{Yp})D + C_{Yv} + \hat{T}_0\,(\partial\bar{x}/\partial s)_a]\,\tilde{\psi} +$$
$$\{C_{Yp}\,D - C_{Yv}\sin\theta_0 + [(\hat{B}-\widehat{mg}) - \hat{T}_0\,(\partial\bar{z}/\partial s)_a]\cos\theta_0 - \hat{T}_0\,(\partial\bar{x}/\partial s)_a\sin\theta_0\}\,\tilde{\varphi} - \hat{T}_0\,(\partial\bar{y}/\partial s)_a = 0 \qquad \text{(A2)}$$

$$\{[(C_{Za3}-\mu)\cos\theta_0 - C_{Za1}\sin\theta_0]\,D^2 + (C_{Zw}\cos\theta_0 - C_{Zu}\sin\theta_0)\,D\}\,\hat{z} +$$
$$\{[C_{Za1}\cos\theta_0 + (C_{Za3}-\mu)\sin\theta_0]\,D^2 + (C_{Zu}\cos\theta_0 + C_{Zw}\sin\theta_0)\,D\}\,\hat{x} +$$
$$\{C_{Zq}\,D - [C_{Zw} + \hat{T}_0\,(\partial\bar{x}/\partial s)_a]\cos\theta_0 - [(\hat{B}-\widehat{mg}) - \hat{T}_0\,(\partial\bar{z}/\partial s)_a]\sin\theta_0\}\,\tilde{\theta} -$$
$$\hat{T}_0\,[(\partial\bar{z}/\partial s)_a\cos\theta_0 + (\partial\bar{x}/\partial s)_a\sin\theta_0] = 0 \qquad \text{(A3)}$$

$$(C_{Ia2}\,D^2 + C_{Iv}D)\,\hat{y} + [(C_{Ia1}-i_{xx})\,D^2 + C_{Ip}\,D - C_{Iv}\sin\theta_0 + \hat{R}\hat{B}\sin\gamma\cos\theta_0]\,\tilde{\varphi} + \{[(i_{xx}-C_{Ia1})\sin\theta_0 + i_{xz}\cos\theta_0]\,D^2 + (C_{Ir}\cos\theta_0 - C_{Ip}\sin\theta_0)\,D + C_{Iv}\}\,\tilde{\psi} = 0 \qquad \text{(A4)}$$

$$[(C_{ma3}\cos\theta_0 - C_{ma1}\sin\theta_0)\,D^2 + (C_{mw}\cos\theta_0 - C_{mu}\sin\theta_0)\,D]\,\hat{z} +$$
$$[(C_{ma1}\cos\theta_0 + C_{ma3}\sin\theta_0)\,D^2 + (C_{mu}\cos\theta_0 + C_{mw}\sin\theta_0)\,D]\,\hat{x} +$$
$$((C_{ma2}-i_{yy})\,D^2 - \{[C_{mw} + \hat{R}\hat{B}\sin\gamma + \hat{R}_a\hat{T}_0\,(\partial\bar{z}/\partial s)_a]\times\cos\theta_0 - [\hat{R}\hat{B}\cos\gamma + \hat{R}_a\hat{T}_0\,(\partial\bar{z}/\partial s)\,a]\times\sin\theta_0\}) - \hat{R}_a\hat{T}_0\,[(\partial\bar{x}/\partial s)_a\sin\theta_0 + (\partial\bar{z}/\partial s)_a\cos\theta_0] = 0 \qquad \text{(A5)}$$

$$(C_{na2}\,D^2 + C_{nv})D)\,\hat{y} + \{[(C_{na3}-i_{zz})\cos\theta_0 + i_{xz}\sin\theta_0]\,D^2 + (C_{nr}\cos\theta_0 - C_{np}\sin\theta_0)\,D + [C_{nv} - \hat{R}_a\hat{T}_0\,(\partial\bar{x}/\partial s)_a]\}\,\tilde{\psi} +$$
$$\{i_{xz}\,D^2 + C_{np}\,D + [\hat{R}\hat{B}\cos\gamma + \hat{R}_a\hat{T}_0\,(\partial\bar{z}/\partial s)_a]\cos\theta_0 - [C_{nv} - \hat{R}_a\hat{T}_0\,(\partial\bar{x}/\partial s)_a]\sin\theta_0\}\,\tilde{\varphi} + \hat{R}_a\hat{T}_0\,(\partial\bar{y}/\partial s)_a = 0 \qquad \text{(A6)}$$

where $\hat{B}$ = nondimensional body buoyancy force; $\widehat{mg}$ = nondimensional body weight; C_x, C_y, C_z = aerodynamic force coefficients; C_l, C_m, C_n = aerodynamic moment coefficients; $i_{xx}, i_{yy}, i_{zz}, i_{xz}$ = nondimensional body inertias; $\hat{R}$ = nondimensional distance from the body mass center to the body buoyancy center; $\hat{R}_a$ = nondimensional distance from the body mass center to the cable attachment point; s = cable length coordinate; $\hat{T}_0$ = nondimensional cable tension at the attachment point; $\hat{x},\hat{y},\hat{z}$ = nondimensional perturbations of the body's coordinates; $\bar{x},\bar{y},\bar{z}$ = cable equilibrium coordinates at the attachment point; $\check{x},\check{y},\check{z}$ = cable perturbed coordinates at the attachment point; γ = angle between $\mathbf{R}$ and $\mathbf{R}_a$ as shown in Fig. 2; θ_0 = equilibrium angle between ground and $\mathbf{R}_a$; $\tilde{\varphi},\tilde{\theta},\tilde{\psi}$ = perturbed Eulerian angles of the body; and the subscripts $(\,)_a$ = reference to the attachment point; $(\,)_{a1}, (\,)_{a2}, (\,)_{a3}$ = derivatives with respect to the nondimensional linear acceleration components, $\hat{a}1$, $\hat{a}2$, and $\hat{a}3$; $(\,)_{\alpha 1}, (\,)_{\alpha 2}, (\,)_{\alpha 3}$ = derivatives with respect to the nondimensional angular acceleration components, $\alpha 1$, $\alpha 2$, and $\alpha 3$; $(\,)_p, (\,)_q, (\,)_r$ = derivatives with respect to the nondimensional angular velocity components, $\hat{p}$, $\hat{q}$, and $\hat{r}$; $(\,)_u, (\,)_v, (\,)_w$ = derivatives with respect to the nondimensional velocity components, $\hat{u}$, $\hat{v}$, and $\hat{w}$.

References

[1] Bairstow, L., Relf, E. F., and Jones, R., "The Stability of Kite Balloons: Mathematical Investigation," R and M 208, Dec. 1915, Aeronautical Research Council, National Physical Lab., Teddington, Middlesex, England.

[2] Berg, P. W. and McGregor, J. L., "The Method of Eigenfunction Expansions," *Elementary Partial Differential Equations*, preliminary ed., Holden-Day, San Francisco, 1964, pp. 72–76.

[3] Bryant, L. W., Brown, W. S., and Sweeting, N. E., "Collected Researches on the Stability of Kites and Towed Gliders," R and M 2303, Feb. 1942, Aeronautical Research Council, National Physical Lab., Teddington, Middlesex, England.

[4] DeLaurier, J. D., "A First Order Theory for Predicting the Stability of Cable Towed and Tethered Bodies where the Cable has a General Curvature and Tension Variation," VIK TN 68, March 1971, von Kármán Inst. for Fluid Dynamics, Rhode-Saint-Genese, Belgium.

[5] DeLaurier, J. D., A Stability Analysis of Cable-Body Systems Totally Immersed in a Fluid Stream," SUDAAR 411, Aug, 1970, Stanford Univ., Stanford, Calif.

[6] Etkin, B., "General Equations of Unsteady Motion," *Dynamics of Flight*, 5th ed., Wiley, New York, 1966, p. 133.

[7] Glauert, H., "The Stability of a Body Towed by a Light Wire," R and M 1312, Feb. 1932, Aeronautical Research Council, National Physical Lab., Teddington, Middlesex, England.

[8] Haak, E. L., "Wind Tunnel Test Results—Family II-D Aerodynamically Shaped Balloon," SER 0093, March 1971, G. T. Schjeldahl Co., Northfield, Minn.

[9] Hoerner, S. F., "Pressure Drag," *Fluid Dynamic Drag*, 1965 ed., Hoerner, Midland Park, N.J., 1965, pp. 3–11.

[10] Maryniak, J., "Simplified Longitudinal-Stability Analysis for a Glider in Towed Flight," *Mechanika Teoretyczna i Stosowana*, Vol. 5, No. 1, May 1967, pp. 57–101.

[11] Munk, M. M., "Aerodynamics of Airships," *Aerodynamic Theory*, Vol. VI, edited by W. F. Durand, 1st ed., Springer, Berlin, 1936, pp. 32–48.

[12] Redd, T, L., Bennet, R. M., and Bland, S.R., "An Analysis and Trend Study of the Stability of a Balloon Tethered in a Wind, with Experimental Comparison," NASA TN, Langley Research Center, Hampton, Va., to be published.

[13] Etkin, B., "The Stability Derivatives," *Dynamics of Flight*, 5th ed., Wiley, New York, 1966, pp. 145–175.